Supplementary Material

Abbreviations: TGF-β, transforming growth factor type β; $O_2^{\bullet-}$, superoxide; $NO^{\bullet}$, nitric oxide; HOCl, hypochlorous acid; H_2O_2, hydrogen peroxide; $^{\bullet}OH$, hydroxyl radicals; $ONOO^-$, peroxynitrite anion; ONOOH, peroxynitrous acid; POD, peroxidase; MPO, myeloperoxidase; MPO-I, myeloperoxidase compound I; GSH, glutathione (reduced form); LPO, lipid peroxidation; NAME, N-omega-Nitro-L-arginine methylester hydrochloride; NMMA, N6-Methyl-L-arginine; SIN-1, 3-morpholino-sydnonimine; GOX, glucose oxidase; Tau, taurine; Ter, terephthalate; NADPH oxidase, nicotinamide adenine dinucleotide phosphate-oxidase; PBS, phosphate buffered saline; XA, xanthine; XO, xanthine oxidase

I. Biochemical reactions involved in intercellular signalling

The list of species involved in the HOCl pathway of intercellular induction of apoptosis modelled in this work is given in Table II, together with their diffusion coefficients. As illustrated for superoxide, somewhat differing values of diffusion coefficients are found in the literature. Nevertheless, potential under- or overestimations of diffusion coefficients D_A can be compensated by lifetimes t_A of the species, as the model results are influenced primarily through the product $D_A t_A$.

Table II: Chemical species involved in the HOCl signalling pathway and their diffusion properties

Species	Diffusion coefficient D (10^{-9} m^2s^{-1})	Note
$O_2^{\bullet-}$	2.8	Ref.26; 1.75 in ref.27, 5.0 in ref.20
H_2O_2	2.3	Ref.27
Peroxidase (myeloperoxidase, MPO)	0.07	Ref.28
HOCl	2.7	Ref.29
$^{\bullet}OH$	2.2	Ref.27

Chemical reactions involved in the HOCl pathway are listed in Table III. The peroxidase cycle has been represented by reactions 2-5 (cf. refs.30,31,32). The kinetic data for two redox states of myeloperoxidase, native (MPO) and compound I (MPO-I), have been employed not only for reconstitution experiments in which MPO was actually used, but also as surrogates for the unknown reaction kinetics of the peroxidase domain of dual oxidase (DUOX) involved in intercellular signalling leading to apoptosis. Thus, potential differences in reaction kinetics between different peroxidases (cf. ref.33) have been neglected; the peroxidase release rates reported in this work thus have to be considered as MPO-equivalent ones.

Table III: Reactions involved in the HOCl pathway of intercellular signalling

No.	Reaction	Rate constant k ($M^{-1}s^{-1}$)	Note
1	$2\ O_2^{\bullet-} + 2\ H^+ \rightarrow H_2O_2 + O_2$	2.0×10^5	Refs.30,4; 4.0×10^5 in ref.34; $d[O_2^{\bullet-}]/dt = -2k[O_2^{\bullet-}]^2$
2	$MPO + H_2O_2 \rightarrow MPO\text{-}I$	2.6×10^7	Ref.30 and refs. therein
3	$MPO\text{-}I + H_2O_2 \rightarrow MPO + O_2 + H_2O$	2.0×10^6	Ref.30 and refs. therein
4	$MPO\text{-}I + Cl^- \rightarrow MPO + HOCl$	$2.5\text{x}10^4$	Ref.30 and refs. therein
5	$MPO + HOCl \rightarrow MPO\text{-}I + Cl^-$	$2.4\text{x}10^7$	Ref.32 for horseradish peroxidase
6	$HOCl + O_2^{\bullet-} \rightarrow {}^{\bullet}OH + Cl^- + O_2$	7.5×10^6	Ref.35 and refs. therein
7	$H_2O_2 + HOCl \rightarrow H_2O + O_2 + H^+ + Cl^-$	1.0×10^5	Ref.14 and refs. therein
8	$^{\bullet}OH$ + lipid → initiation of lipid peroxidation	10^9	Refs.15,36 and refs. therein

II. Numerical solution of the model and analytical approximations used

The given coupled set of partial differential equations has been implemented in dedicated computer codes written in FORTRAN. The codes were run on a high-end linux-based PC. Differential equations have been replaced by their difference analogues, with concentration profiles represented on a discrete voxel and time step grid. Voxel sizes and time steps have been taken so as to fulfil the stability criterion for diffusion equation (37) and to keep the changes of species concentrations in each time step much smaller than the current concentrations. Independence of the resulting apoptosis kinetics on voxel size and time step has been required, too. To reduce computational expensiveness, voxel sizes and time steps have been enlarged for longer-living species, and correspondingly larger time steps have been used for cell densities that change relatively slowly compared to species' lifetimes. First-order Euler method has been used for numerically solving the given difference equations, $f(t + \Delta t) = f(t) + \Delta t\, \partial f/\partial t$.

Furthermore, approximations have been introduced for processes that involve short-lived species and are very fast, namely for individual reactions of the peroxidase cycle, for reactions producing HOCl and $^{\bullet}$OH, and for the absorption of apoptotic inducers after having attacked the cells. For such a short-lived species (denoted by A), a (spatially varying) quasi-steady state is quickly reached in which local concentration [A](z,t) is given by the balance of production and absorption reactions; diffusion can be neglected with respect to reactions and disappearance due to the short lifetime. For intermediate times much larger than species' lifetime t_A but much shorter than lifetimes of relatively long-lived species, equation (1) in this local steady-state approximation takes the form of

(S1) $[A](z,t)/t_A = \Sigma_{C,D}\, k_{C+D\rightarrow A+B}\, [C](z,t)\, [D](z,t) - \Sigma_{B}\, k_{A+B\rightarrow C+D}\, [A](z,t)\, [B](z,t)$

For HOCl, this local quasi-steady-state approximation leads to

(S2) $[HOCl](z,t) = k_4\, [MPO\text{-}I](z,t)[Cl^-] / ((t_{HOCl})^{-1} + k_6\, [O_2^{-\bullet}](z,t) + k_7\, [H_2O_2](z,t) + k_5\, [MPO](z,t))$

where k_i stand for the reaction rate of the i-th reaction in Table III.

Also the peroxidase cycle (reactions 2-5 in Table III) has been represented in local quasi-steady-state approximation. Diffusive motion has been considered for the sum of different redox states of the enzyme. Branching into the redox states has been simulated then on a voxel-specific basis, considering the spatially-dependent availability of different peroxidase substrates and reaction partners (H_2O_2, Cl^- and HOCl, cf. Table III).

A similar approach has been used for $^{\bullet}$OH too. However, even with this quasi-steady-state approximation, an explicit representation of the absorption of apoptosis-inducing $^{\bullet}$OH after attacking the cells and initiating lipid peroxidation in their membranes would be tremendously computationally expensive due to the extremely short lifetime of $^{\bullet}$OH (~μs), which translates into the need for taking very small voxels. To solve this issue, an analytical formula describing this absorption, obtained as a homogeneous solution of the corresponding kinetic equation for $^{\bullet}$OH, equations (1)-(2), has been added to its particular solution obtained from numerical simulations that do not account for this absorption.

The mentioned approximations have been benchmarked against full numerical simulations (results not shown). With these approximations, 0.2 – 20 h computing time on a high-end linux-based PC is needed to simulate the system over the time span of 10 d. The computational expensiveness depends critically on the voxel and time step sizes used. Generally, increased release rates of primary species require using smaller steps to keep the same calculation precision, as the role of mutual reactions increases with respect to non-specific absorption described by the species' lifetime. Shorter lifetimes also translate into the need of using smaller time steps.

III. Model calibration

Additional results of model calibration against data from experiments with externally added species, complementing those presented in Figure 2 in the main text, are shown in Figure 5.

Unless stated otherwise, modelling based on homogeneous chemistry is used, as the externally added species dominate over cell-derived ones. The approaches used for individual systems reported in Figure 2 and Figure 5 are given below.

1. Apoptosis induced by $^{\bullet}OH$ from decay of peroxynitrite generated by its donor SIN-1. 3-morpholino-sydnonimine (SIN-1) decays by a three-step mechanism (38) that consists of (i) opening the sydnonimine ring to SIN-1A, (ii) reduction of O_2 to $O_2^{-\bullet}$ by SIN-1A yielding radical cation SIN-$1^{\bullet+}$, and (iii) decomposition of SIN-$1^{\bullet+}$ into SIN-1C and $NO^{\bullet}$. Detailed simulations representing this three-step mechanism as well as dismutation of $O_2^{-\bullet}$ into H_2O_2 have verified that, within the parameter region of interest in this study, virtually all $O_2^{-\bullet}$ react with $NO^{\bullet}$ to yield $ONOO^-$, giving almost 1:1 molar ratio between the amount of SIN-1 used and ONOO- produced (not shown; similar results reported in refs.39,40 and refs. therein). These simulations have also shown that the three-step mechanism of SIN-1 decay can be approximated by a simplified, two-step decay scheme, considering a ring opening step with characteristic time $t_{\text{SIN open}}$ and a single decay step in which $ONOO^-$ is produced directly, with characteristic time $t_{\text{SIN decay}}$; an analogous scheme has been used e.g. in ref.(41).

In the analyzed experiments, SIN-1 dissolved in phosphate buffered saline (PBS) was added, either directly or after 1–2 h preincubation in PBS, at various final concentrations to the cell culture medium; apoptosis was scored after 1–7 h (14). Neglecting potential differences between decay rates of SIN-1 (and peroxynitrite) in PBS and in culture medium, the two-step decay of SIN-1 into peroxynitrite and decay of peroxynitrite into $^{\bullet}OH$ can be solved analytically in the quasi-steady-state approximation ($t_{OH} << t_{ONOO} << \min(t_{\text{SIN open}}, t_{\text{SIN decay}})$), yielding

(S3) $$[^{\bullet}OH](t)=[\text{SIN-1}]_0(\exp(-t/t_{\text{SIN open}})-\exp(-t/t_{\text{SIN decay}}))\eta_{OH}\, t_{OH}/(t_{\text{SIN open}}-t_{\text{SIN decay}})$$

where $[\text{SIN-1}]_0$ is the concentration of SIN-1 added (accounting for the corresponding dilution factor when added to the medium), and η_{OH} denotes the efficiency of $^{\bullet}OH$ formation ($\eta_{OH} \sim 30$ %; $NO_3^- + H^+$ are formed in the other ~ 70 % of cases, cf. ref.42). Parameters $t_{\text{SIN open}}$ and $t_{\text{SIN decay}}$ have been treated as adjustable parameters. Note that in this approximation, $^{\bullet}OH$ yields are independent of peroxynitrite lifetime in the medium[*] t_{ONOO}. Absorption of $^{\bullet}OH$ due to initiating lipid peroxidation has been accounted for as described above.

2. Synthetic H_2O_2. The amount of hydrogen peroxide present in the medium is determined by first-order decay kinetics with lifetime t_{H2O2}. Initiation of lipid peroxidation by H_2O_2 has been approximated by the effective reaction rate constant $k_{\text{LPO H2O2}}$. Absorption of H_2O_2 due to LPO is considered in a way analogous to that used for $^{\bullet}OH$; however, as $k_{\text{LPO H2O2}}$ is much smaller than $k_{\text{LPO OH}}$, also the reduction of $[H_2O_2]$ in the vicinity of cells is smaller than for $[^{\bullet}OH]$, though farer ranging due to longer lifetime.

3. H_2O_2 generated by glucose oxidase. In this case, H_2O_2 is gradually produced from oxygen and glucose (abundant in the culture medium) by glucose oxidase (GOX). The rate of H_2O_2 production has been assumed to be constant, given by the amount of the enzyme present. Under optimal conditions, 1 U of the enzyme converts 1 μmol substrate per 1 min; a single calibration factor η_{GOX} has been introduced to account for the sub-optimal efficiency of GOX under the given experimental conditions, indicated by the ratio of apoptotic responses to synthetic and GOX-generated H_2O_2 (14).

---

[*] While peroxynitrite anion ONOO- is relatively stable in water solution in the absence of further reaction partners, its protonated form, peroxynitrite acid ONOOH, pKa = 6.8, decomposes spontaneously with $t_{ONOOH} \sim 1$ s at 37°C and pH 7.4 (36), so that at pH 7.4 the lifetime of ONOO-/ONOOH is 4.17 s (43).

4. H_2O_2 generated from superoxide produced by xanthine oxidase. Superoxide has been assumed to be produced by xanthine oxidase at a constant rate until the enzyme uses up all available substrate (0.0004 mM xanthine, ref. 14). No additional calibration factor for enzyme efficiency has had to be introduced. Superoxide was allowed to disappear in non-specific reactions with medium constituents (with lifetime $t_{O2\text{-}\bullet}$) and spontaneously dismutate, gradually producing H_2O_2.

5. HOCl produced by myeloperoxidase from H_2O_2 generated by glucose oxidase. Winterbourn et al. (30) and Jakopitch et al. (32) have gathered detailed information on myeloperoxidase (MPO) reaction kinetics, listed in Table III. To be able to make use of this information in the analysis of experiments on apoptosis induction (14), in which the amounts of MPO used are given in enzyme units (U), conversion factors between enzyme units and moles have to be determined first. 1 U of MPO is defined by producing, in a spectrophotometric assay of the oxidation of guaiacol in 50 mM potassium phosphate buffer with 100 mM guaiacol and 0.0017 % (w/w) hydrogen peroxide at pH 7.0 and 25°C, an increase in absorbance at 470 nm of 1.0 per minute at pH 7.0 and 25°C, in total reaction volume of 3.035 ml (44). Upon oxidation, guaiacol forms tetraguaiacol; an increase in tetraguaiacol concentration of 1 mM leads to an increase in absorbance at 470 nm of 26.6 (45). Hence, the required increase in absorbance at 470 nm of 1.0 in the myeloperoxidase assay corresponds to the formation of 1 mM / 26.6 × 3.035 ml = 0.114 μmol of tetraguaiacol by 1 U of MPO in 3.035 ml reaction volume per minute.

The kinetics of guaiacol oxidation by MPO with H_2O_2 has been studied experimentally by Capeillère-Blandin (46). Assuming a minimal representation of guaiacol (G-OH) reactions with the MPO/H_2O_2 system,

MPO + H2O2 → MPO-I ($k_{G1} = 6 \times 10^6$ $M^{-1}s^{-1}$ or 2.6×10^7 $M^{-1}s^{-1}$, ref. 46 or 30)

MPO-I + G-OH → MPO + G-O$^\bullet$ ($k_{G3} = 3.5 – 5.3 \times 10^4$ $M^{-1}s^{-1}$, ref. 46)

MPO-I + H2O2 → MPO ($k_{G2} = 2 \times 10^6$ $M^{-1}s^{-1}$, ref. 30)

leads under quasi-steady-state approximation ([MPO] ~ const, [MPO-I] ~ const) to kinetics of guaiacol oxidation of Michaelis-Menten type,

$$v/E_0 = k_{G1}\, k_{G3}\, [H_2O_2]\, [G] / (k_{G3}\, [G] + (k_{G1} + k_{G2})\, [H_2O_2]) ,$$

where E_0 is the total amount of MPO and [G] denotes guaiacol concentration. We have tested (results not shown) that this formula is in agreement with detailed data on the rate of guaiacol oxidation by the MPO/H_2O_2 system in dependence of both guaiacol and H_2O_2 concentrations, measured by Capeillère-Blandin (46). Extrapolations to the experimental conditions of the peroxidase assay, 100 mM guaiacol and 0.5 mM (i.e., 0.0017 % w/w) H_2O_2, yield the rate of guaiacol oxidation (formation of G-O$^\bullet$) $v/E_0 = 1.5 \times 10^3$ s^{-1}.

Assuming that the formation of tetraguaiacol from four G-O$^\bullet$ molecules is fast, 1 U of MPO producing 0.1141 μmol tetraguaiacol per minute translates into 0.4564 μmol/min = 7.6 nmol/s G-O$^\bullet$. Comparison with the rate of guaiacol oxidation above, $v/E_0 = 1.5 \times 10^3$ s^{-1}, gives the sought conversion factor, 1 U = 5 pmol MPO.

In the reconstitution experiments on apoptosis induction by the H_2O_2/MPO system (14), H_2O_2 was continuously generated by glucose oxidase, and then used by MPO to produce HOCl from Cl^- abundant in the culture medium ([Cl^-] ~ 0.1 M). All these processes are homogeneous in space. However, apoptosis-inducing $^\bullet$OH were produced then in the reaction of HOCl with superoxide produced by transformed cells. Due to short lifetime (and hence short diffusion length) of superoxide, homogeneous chemistry cannot be employed for this step; thus, detailed numerical simulation of the reaction scheme has been used as described for intercellular signalling in the previous section. Consumption of HOCl in reaction with H_2O_2 (Table III) has been included too.

In modelling the experiments (14) with taurine which is a scavenger of HOCl, the HOCl lifetime was reduced according to the added amount of the scavenger (50 mM) and its reaction rate with HOCl, $(5 – 16) \times 10^5$ $M^{-1}s^{-1}$ (ref.47,48). Similarly, for terephthalate which

scavenges •OH, the amount of terephthalate added (0.2 mM) and its reaction rate with •OH (3.3×10^9 $M^{-1}s^{-1}$, ref.49) have led to a reduced lifetime of •OH in the medium, $1/t'_{OH} = 1/t_{OH} + k_{terephthalate + \bullet OH}$ [terephthalate], the second term limiting the lifetime of •OH under the presence of terephthalate to ≤ 1.5 µs. The standard lifetime of •OH in the medium t_{OH} used throughout the simulations, 3.4 µs (Table I), is a model estimate which reflects the high reactivity of •OH and, on the other hand, the fact that this concentration of terephthalate completely diminished apoptosis induction (Figure 2 and ref.14), so that the lifetime of •OH in the absence of terephthalate must have been somewhat longer than 1.5 µs. The given value (3.4 µs) is, however, related also to the values of other model parameters, as discussed below.

Table IV: Estimates of model parameters involved in the reported calibration studies; parameters relevant also for intercellular induction of apoptosis are reported in Table I in the main part of the paper.

	Parameter	Value
$t_{open\ SIN}$	Characteristic time of SIN-1 ring opening (h)	1.68
t_{SIN}	Characteristic time of SIN-1 decay (s)	0.71
η_{GOX}	Efficiency of glucose oxidase (%)	6.8
$k_{H2O2\ LPO}$	Effective reaction rate constant for lipid peroxidation by H_2O_2 ($M^{-1}s^{-1}$)	0.022

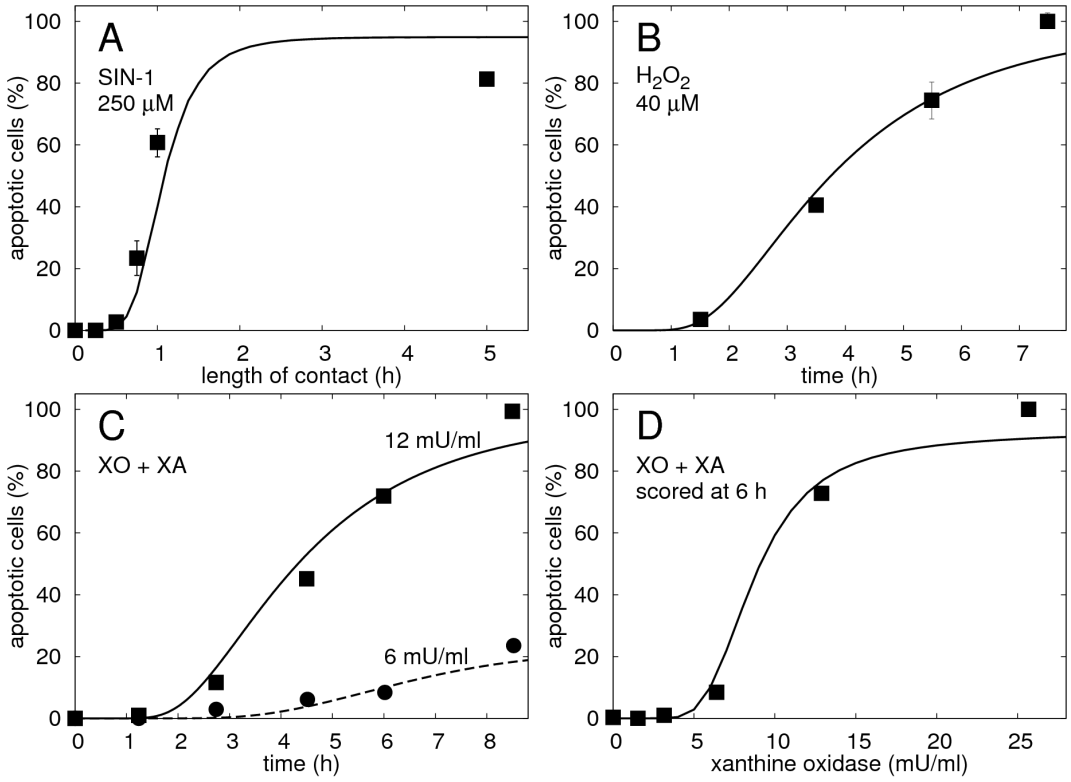

Figure 5: Apoptosis induced in 208F src3 transformed rat fibroblasts by external donors of key signalling species involved in intercellular induction of apoptosis: Further results complementing Figure 2. Calibration of model calculations (lines) against data (points, errorbars denoting standard errors of the mean from several repeats of the experiment, from ref.14; where not shown, were the errorbars smaller than the symbols). (A) Percentage of apoptotic cells in dependence on the length of exposure to peroxynitrite donor SIN-1; medium with SIN-1 removed at indicated times, replaced by fresh one, and apoptosis scored at 7 h total time. (B) Kinetics of apoptosis induction by 40µM H_2O_2. (C) Apoptosis induced by H_2O_2 from dismutation of superoxide, generated by 6 or 12 mU/ml xanthine oxidase (XO) from 0.4 mM xanthine (XA) added to medium. (D) Concentration dependence of apoptosis induction by this system.

IV. Detailed characteristics of the signalling mechanism predicted by the model

To illustrate the behaviour of the HOCl pathway of intercellular induction of apoptosis in greater detail, the results presented in Figure 3 are complemented by further ones in Figure 6. In the analyzed co-culture experiments (11), 40000 non-transformed cells were seeded per 9.6 cm^2 well and pre-treated with TGF-β for 2 days. Transformed cells were seeded at the same density, 20 h before start of co-culture. Cell proliferation during these periods has been accounted for; thus the starting densities at the beginning of co-culture (t = 0 in model calculations) are correspondingly higher than the initial seeding density of ~ 42/mm^2 (Figure 6A). Within the first ~1.7 d, the density of living (i.e., non-apoptotic) transformed cells increases by proliferation but is then reduced (up to ~2.7 d) via induction of apoptosis, and then slightly increases as proliferation again dominates over apoptosis (Figure 6A); a few damped oscillations follow (cf. Figure 3B). As apoptosis induction in non-transformed cells is negligible, their density steadily increases towards the saturation value (confluence) assumed at 200/mm^2 (Figure 6A).

The three vertical lines in Figure 6A indicate three time points at which concentration profiles of the major signalling species have been scored and plotted in Figure 6B-F in dependence on the distance, z, from the transformed cells' plate. The time points correspond (Figure 6A) to the initial signalling phase (at 0.5 d after the start of co-culture) and to the maximal and minimal density of transformed cells (at 1.7 or 2.7 d, respectively). With increasing density of transformed cells, superoxide concentrations increase (Figure 6B, green vs. red line). More importantly, $O_2^{-\bullet}$ concentrations rapidly fall off with increasing distance from its source, the transformed cells; the reduction (by about 6 orders of magnitude per 1 mm) is dominantly influenced by limited superoxide lifetime (estimated as 1.7 s, Table I). The long-lived peroxidase (lifetime 10^6 s) released by effector cells (located at 1mm distance from transformed cells) gradually accumulates, and is distributed almost homogeneously (Figure 6C). H_2O_2 produced by dismutation of $O_2^{-\bullet}$ has a limited range (Figure 6D); this is partially due to the rapid fall off in superoxide concentrations but mainly due to consumption of H_2O_2 by peroxidase. Indeed, at 0.5 d the H_2O_2 concentration is reduced by factor of 2 per 150μm increase in distance from transformed cells (i.e. by about 2 orders of magnitude per 1 mm, Figure 6D blue line), while at later times under higher amounts of peroxidase this reduction increases to factor of 5 per 150 μm (more than 4 orders of magnitude per 1 mm; Figure 6D red line). Concentration profiles of HOCl (Figure 6E) follow the same shape as H_2O_2, as the yields of HOCl are directly proportional to MPO-I (Table III), whose amounts are proportional to local concentrations of H_2O_2 and peroxidase. The slight shift in HOCl concentrations at transformed cells (as compared to H_2O_2 levels) follows from accumulation of peroxidase in the medium.

The calculated profiles of apoptosis-inducing $^{\bullet}OH$ (Figure 6F) fall off with distance from transformed cells even faster, combining the fall-offs of HOCl and $O_2^{-\bullet}$ that have to react to produce $^{\bullet}OH$ (Table III). In addition, due to absorption of $^{\bullet}OH$ upon attacking the cells and initiating lipid peroxidation (LPO) in their membranes, in a very close vicinity of transformed (and effector) cells the $^{\bullet}OH$ concentration is further reduced, by about a factor 10; the short range of this effect is given by the extremely short lifetime of $^{\bullet}OH$ which prevents this absorption effect from propagating farer. This absorption actually slightly depends on cell density, cf. equation (2). In Figure 6G, this effect is illustrated and model predictions for $^{\bullet}OH$ yields at transformed and normal cells are shown. While the predicted levels of $^{\bullet}OH$ at transformed cells follow the density of transformed cells (with a delay of about 1.5 h), the levels of $^{\bullet}OH$ at 1mm distant non-transformed cells are predicted to decrease with time, mainly due to the build-up of peroxidase levels and hence reduction of HOCl concentrations at that place as discussed above.

As shown in Figure 6H, the amount of LPO damage follows the kinetics of $^{\bullet}OH$ levels, with a delay of about 8 h which reflects the cellular capacity to repair LPO damage (t_{rep}=15 h,

Table I). The LPO levels in co-culture experiments are predicted to result almost completely from $^{\bullet}OH$ attacks (this contribution, neglecting LPO induction by H_2O_2, is shown by green line in Figure 6H). Furthermore, LPO levels are predicted to stay below the characteristic level n_1 for apoptosis induction (10^{-17} mol/cell, Table I, dashed line in Figure 6H), reaching only about 75 % of this value, corresponding to the rate of apoptosis induction of only 10 % of the maximal rate (i.e., $p_{ind} \leq 0.1$ in equations (3)-(4)). This explains why apoptosis induction in co-culture experiments is much slower compared to experiments with external donors of signalling species, e.g. the GOX system (Figure 6H, blue line), in which the characteristic level n_1 for apoptosis induction is rapidly exceeded and apoptosis is induced at its maximal rate $1/t_{ind}$.

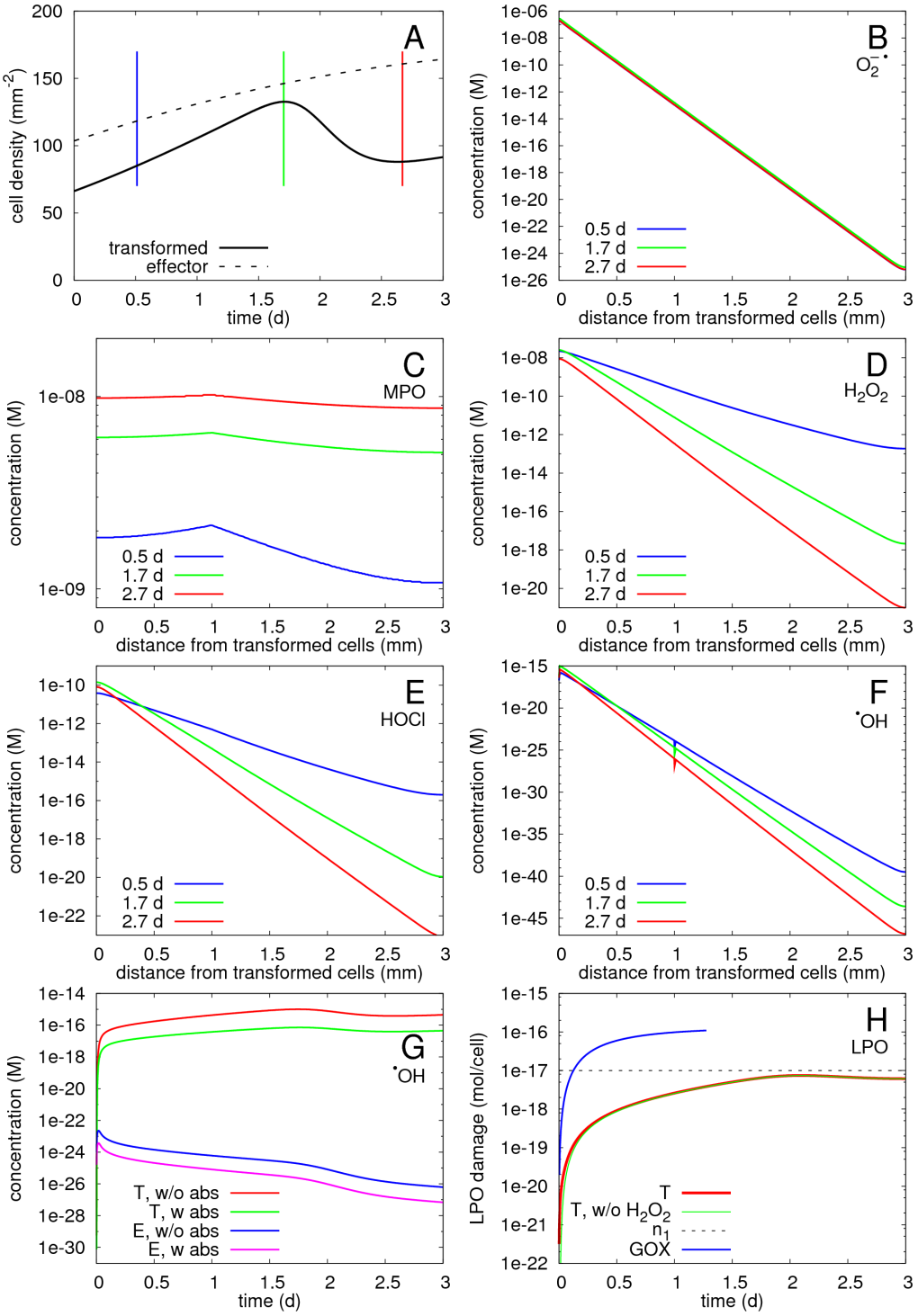

Figure 6: Detailed characteristics of the HOCl signalling pathway leading to the induction of apoptosis, complementing results shown in Figure 3A. (A) Density of living (i.e., non-apoptotic) transformed (solid line) and normal cells (dashed line). (B-F) Concentration profiles of signalling species at time points indicated by vertical lines in (A): at 0.5 d after the start of co-culture (blue), at maximal and minimal density of transformed cells (~1.7 d or ~2.7 d, green and red lines, respectively). (G) Temporal development of $^{\bullet}OH$ concentrations at the surface of transformed cells without (red) or with accounting for absorption of apoptosis inducers upon attacking the cells (green line); model predictions for normal cells shown too (blue and pink line, respectively). (H) The amount of unrepaired LPO damage in transformed cells (red line), contribution from $^{\bullet}OH$ attacks (i.e., without LPO induction by H_2O_2, green line). For comparison, LPO induction by external H_2O_2 generated by the GOX system (Figure 2C) is shown (blue line), together with the characteristic level of LPO triggering apoptosis (10^{-17} mol/cell, Table I; dashed line).

V. Parameter identifiability and sensitivity issues

The values or estimates of model parameters used in this work are taken from four sources: First, several model parameters are taken from experimental observations and experience, especially doubling times and confluence densities (Methods). Second, diffusion coefficients and reaction rate constants are taken from the literature; their values are listed in Table II and Table III. Third, lifetimes t_A of signalling species A, cellular sensitivity to apoptosis inducers n_1 and n_2 and the (maximal) rate of apoptosis induction $1/t_{ind}$ are determined from model calibration to experiments with external addition of signalling species (Figure 2 and Figure 5), and listed in Table I. Finally, cellular release rates of primary signalling species and the rates $1/t_{rep}$ of repairing LPO and $1/t_{rm}$ of removing apoptotic bodies are adapted to data from co-culture system with transformed and normal cells.

The data (14) from reconstitution experiments with externally added species are limited to rather short times (typically up to 8 – 12 h, and up to 28 h for the MPO system, cf. Figure 2 and Figure 5), so that no specific information can be derived on the t_{rm} and t_{rep} parameters. Their values of 12 h or more yield equally good results if other parameters are adjusted accordingly. On the other hand, values below 24 h are required to reproduce the data (11) on intercellular induction of apoptosis under co-culture setup (Figure 3). If not specified otherwise, the results shown in this paper correspond to $t_{rm} = t_{rep} = 15$ h. If these processes were not taken into account ($t_{rep} \to \infty$, $t_{rm} \to \infty$), steadily increasing percentages of apoptotic cells would result, and finally the whole transformed cell population would exhibit apoptosis, contrary to the data.

The calibration calculations have also revealed that the cellular sensitivity parameter n_1 scales directly with the effective rate constant $k_{LPO\text{-}H2O2}$ for LPO induction by H_2O_2, and affects the derived $^{\bullet}OH$ lifetime, t_{OH} (not shown). The reported results correspond to the characteristic amount of LPO damage triggering apoptosis $n_1 = 10^{-17}$ mol/cell, which amounts to about 1 % of membrane lipids susceptible to inducer attacks ($n_{lip} \sim 10^{-15}$ mol/cell, ref.16); values of $n_1 = 10^{-18}$ to 10^{-16} mol/cell could be brought into agreement with the data if $k_{LPO\text{-}H2O2}$ and t_{OH} are scaled accordingly (not shown). Note that only LPO initiation events are scored here; the actual fraction of damaged lipids in cell membrane is likely enhanced by LPO propagation reactions (cf.17,18).

Furthermore, the per-cell release rate of superoxide, $\alpha_{O2^{-\bullet}}$, and lifetime of HOCl, t_{HOCl}, which are reflected in the GOX + MPO system (Figure 2C) only, are mutually correlated; e.g., $\alpha_{O2^{-\bullet}}$ of $(0.2–1)\times10^{-16}$ mol cell^{-1} s^{-1} are consistent with the data if t_{HOCl} is adjusted to 0.25–0.038 s (not shown). However, for given t_{rm}, t_{rep} and n_1, the values of other model parameters can be derived from the data with reasonably small uncertainties. In particular, parameters t_{ind}, $t_{O2^{-\bullet}}$, t_{H2O2} are practically independent of the chosen t_{rm}, t_{rep} and n_1.

Of particular importance is the lifetime of superoxide $t_{O2^{-\bullet}}$, as this is the crucial parameter with respect to the sensitivity of intercellular induction of apoptosis to the transformed phenotype. For *in vitro* conditions, superoxide lifetime (1.7 s) has been derived (cf. Figure 5) by comparing the data on apoptosis induction by superoxide-generating system (xanthine with xanthine oxidase) that yields H_2O_2 via superoxide dismutation with the data on the effects of H_2O_2 (synthetic or enzymatically generated). Choosing alternative values of other parameters has resulted in less than 5% variations in superoxide lifetime under *in vitro* conditions (results not shown). The value assumed for superoxide lifetime *in vivo* (0.1 s) comes from a study on radical signalling in blood (20), and is given mainly by levels of antioxidants such as ascorbic acid.

The above discussion illustrates the fact that although the present model of intercellular induction of apoptosis works with mechanistically distinct parameters, not all of them can be determined unambiguously from the limited set of data; i.e., from the viewpoint of data analyses, the parameters are correlated. Also the adjustment of the cellular release rates of superoxide and peroxidase to the observed kinetics of apoptosis induction in the transformed-

nontransformed coculture system is not unique, although (with other parameters assigned their 'standard values' used throughout the paper) $\alpha_{O2\text{-}\bullet}$>$5\times10^{-16}$ mol cell^{-1} s^{-1} and t_{rm}, t_{rep}<24 h are needed for agreement with the data, putting further restrictions on the values derived from the reconstitution experiments. A few alternative parameter sets consistent with data from both reconstitution and coculture experiments are illustrated in Figure 7A (red line, 'standard parameter set' used in this work: $t_{rm} = t_{rep} = 15$ h, $\sigma^{T}_{max} = 300$ mm^{-2}, $\alpha_{O2\text{-}\bullet} = 10^{-16}$ mol cell^{-1} s^{-1}, $\alpha_{POD} = 10^{-21}$ mol cell^{-1} s^{-1}, $t_{HOCl} = 38$ ms; green line, set 2: as the standard set but $\sigma^{T}_{max} = 200$ mm^{-2}, $\alpha_{POD} = 2\times10^{-21}$ mol cell^{-1} s^{-1}, $t_{HOCl} = 40$ ms; blue line, set 3: as the standard set but $t_{rm} = t_{rep} = 18$ h, $\sigma^{T}_{max} = 200$ mm^{-2}, $\alpha_{O2\text{-}\bullet} = 8\times10^{-17}$ mol cell^{-1} s^{-1}, $\alpha_{POD} = 3\times10^{-21}$ mol cell^{-1} s^{-1}, $t_{HOCl} = 45$ ms; pink line, set 4: as set 3 but $\alpha_{POD} = 5\times10^{-21}$ mol cell^{-1} s^{-1}; light blue line, set 5: as set 3 but $\alpha_{POD} = 10^{-20}$ mol cell^{-1} s^{-1}). However, although alternative parameter sets are consistent with the data, they lead to almost identical predictions for the long-term behaviour of the system, with almost equal long-term limits to transformed cell densities (Figure 7B).

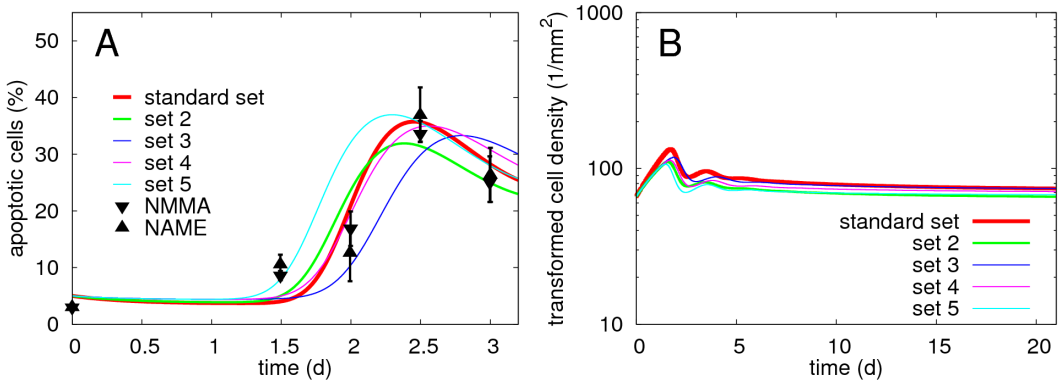

Figure 7: Alternative parameterizations of the model of intercellular induction of apoptosis consistent with the data (11) on kinetics of apoptosis induction in the transformed-nontransformed co-culture system (panel A) lead to almost identical predictions for the long-term system behaviour (panel B). See text for details.

VI. Predicted dependence on experimental setup

Finally, results are reported of a series of simulations aimed at predicting how apoptosis induction in transformed cells through signalling by normal cells via the HOCl pathway is affected by changes in experimental setup. Namely, the effects of the distance between the two co-cultured populations, the amount of medium, and the seeding densities are looked at.

With varying distances between the two co-cultured populations (and keeping other parameters identical, in particular keeping the amount of medium unchanged), the model predicts rather small differences in the rate of apoptosis induction: Apoptosis is predicted to occur a bit faster and in a slightly smaller fraction of cells when the distance between cultures is reduced from 1 mm to 0.5 mm or even 0.1 mm (Figure 8A). In the long term behaviour, there is almost no difference (Figure 8B).

More pronounced effect are predicted when the amount of added culture medium is varied (Figure 8C, medium heights of 4, 3, 2, or 1.5 mm keeping the inter-culture distance at 1 mm). With reduced amount of medium, apoptosis is predicted to occur faster and in a greater fraction of cells, as signalling species (in particular peroxidase) are diluted by diffusion into smaller volumes only. Variations in medium height are predicted to be reflected in the long-term behaviour as well (Figure 8D).

Seeding lower numbers of transformed or non-transformed cells is predicted to delay the onset of apoptosis significantly, but not to have a large effect on the extent of apoptosis (Figure 8E,F). Reducing the number of transformed cells delays the onset of apoptosis more than if fewer non-transformed cells are seeded; this is in line with the crucial role of

transformed cell-derived superoxide in intercellular signalling leading to apoptosis: Sufficient superoxide production, i.e. sufficient transformed cell densities, are needed for intercellular induction of apoptosis being effective. Experimentally, delays in apoptosis induction of about 1 and 2 d were reported (11) for seeding densities reduced to 20000 and 10000 non-transformed cells per well, while the present calculations predict delays of about 4 and 8 h only. Reduced numbers of seeded transformed cells led to a delay of about 1 d too; moreover, the extent of apoptosis was significantly reduced (11), contrary to model predictions. These discrepancies between model calculations and the data may indicate that the second important pathway of intercellular induction of apoptosis, the peroxynitrite pathway, which is not represented in the present calculations, may play an important role in these effects. A detailed discussion of this issue exceeds the scope of this paper.

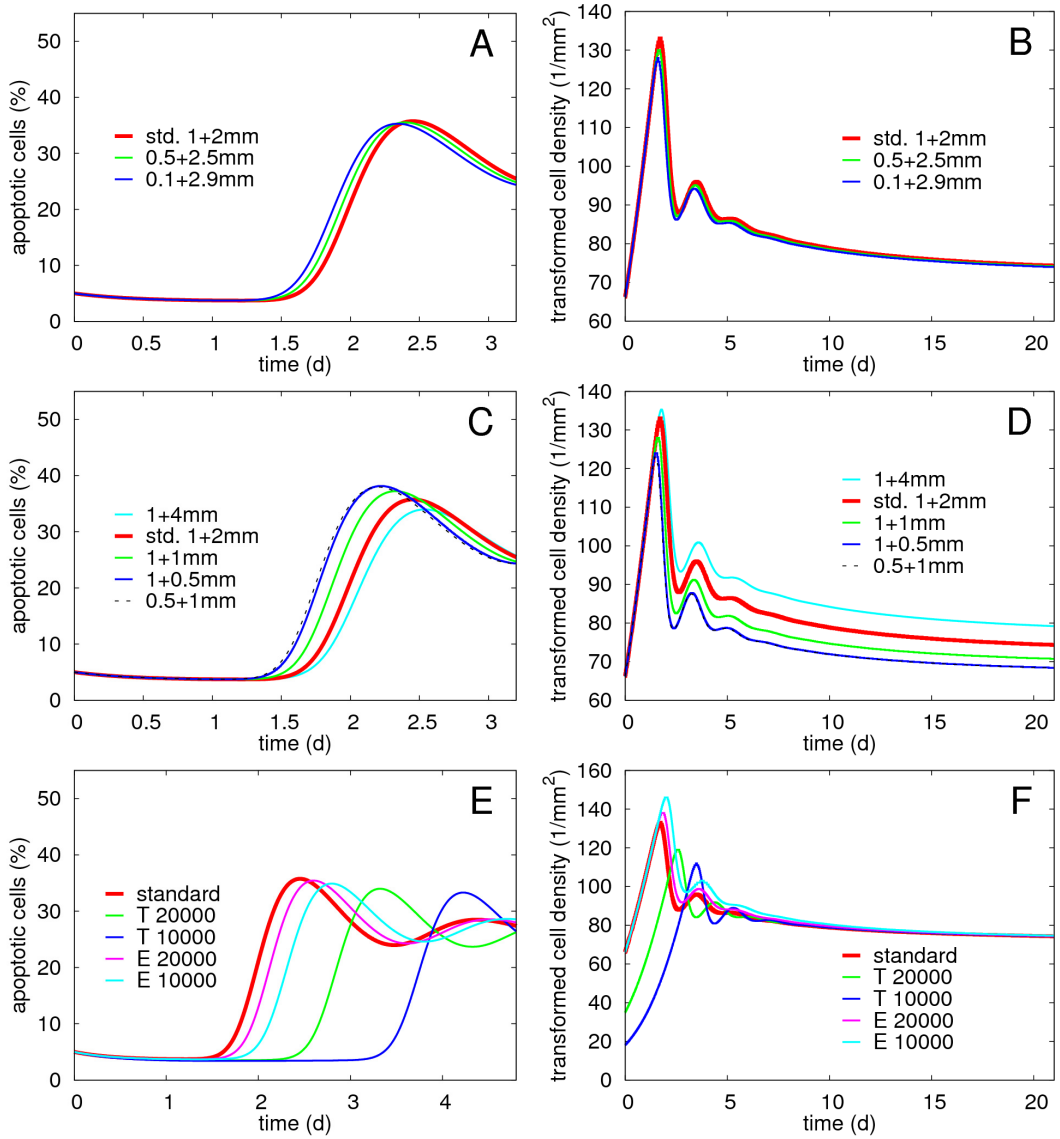

Figure 8: Predicted dependence of intercellular induction of apoptosis via the HOCl pathway on variations in experimental setup. (A, B) The effect of varying the distance between transformed and non-transformed cells, from the standard 1 mm to 0.5 or 0.1 mm, keeping the amount of medium constant (total medium height 3 mm). (C, D) Varying the amount of medium, keeping the distance of the cultures at 1 mm. As in (A), negligible difference is predicted between 0.5 mm distance of the cultures and 1 mm additional medium and the opposite situation (blue and dashed lines). (E, F) Predicted effects of reduced numbers of cells seeded initially. Standard calculation: 40000 transformed cells seeded 20 h before the start of the co-culture experiment, and 40000 non-transformed seeded and pre-treated with TGF-β for 2 d to attain effector function. The model predicts delayed onset of apoptosis when the reported numbers of transformed ('T') or non-transformed effector ('E') cells per 9.6 cm^2 well are reduced to 20000 or 10000.

References

1. Weinberg RA. Oncogenes, Antioncogenes and the molecular basis of multistep carcinogenesis. Cancer Res 1989;49:3713-21.
2. Hanahan D, Weinberg RA. The hallmarks of cancer. Cell 2000;100:57-70.
3. Bauer G. Elimination of transformed cells by normal cells: a novel concept for the control of carcinogenesis. Histol Histopathol 1996;11:237-55.
4. Bauer G. Reactive oxygen and nitrogen species: efficient, selective and interactive signals during intercellular induction of apoptosis. Anticancer Research 2000;20:4115-40.
5. Deichman GI, Early phenotypic changes of in vitro transformed cells during in vivo progression: possible role of the host innate immunity. Semin Cancer Biol 2002;12:317-26.
6. Barcellos-Hoff MH. It takes a tissue to make a tumor: epigenetics, cancer and the microenvironment. J Mammary Gland Biol Neoplasia 2001;6:213-21.
7. Irani K, Xia Y, Zweier JL, Sollott SJ, Der CJ, Fearon ER, et al. Mitogenic signaling mediated by oxidants in Ras-transformed fibroblasts. Science 1997;275:1649-52.
8. Bauer G. Low dose radiation and intercellular induction of apoptosis: potential implications for the control of oncogenesis. Int J Radiat Biol 2007;83:873-88.
9. Bechtel W, Bauer G. Catalase protects tumor cells from apoptosis induction by intercellular ROS signaling. Anticancer Res 2009;29:4541-57.
10. Heinzelmann S, Bauer G. Multiple protective functions of catalase against intercellular apoptosis-inducing ROS signaling of human tumor cells. Biol Chem 2010;391:675-93.
11. Herdener M, Heigold S, Saran M, Bauer G. Target cell-derived superoxide anions cause efficiency and selectivity of intercellular induction of apoptosis. Free Radic Biol Med 2000;29:1260-71.
12. Heigold S, Sers C, Bechtel W, Ivanovas B, Schäfer R, Bauer G. Nitric oxide mediates apoptosis induction selectively in transformed fibroblasts compared to nontransformed fibroblasts. Carcinogenesis 2002;23:929-41.
13. Jürgensmeier JM, Panse J, Schäfer R, Bauer G. Reactive oxygen species as mediators of the transformed phenotype. Int J Cancer 1997;70:587-9.
14. Ivanovas B, Zerweck A, Bauer G. Selective and non-selective apoptosis induction in transformed and non-transformed fibroblasts by exogenous reactive oxygen and nitrogen species. Anticancer Res 2002;22:841-56.
15. Radi R, Turrens JF, Freeman BA. Cytochrome c-catalyzed membrane lipid peroxidation by hydrogen peroxide. Arch Biochem Biophys 1991;288:118-25.
16. Alberts B, Johnson A, Lewis J, Raff M, Roberts K, Walter P. Molecular Biology of the Cell (4th edition), Chapter 10 Membrane Structure - The Lipid Bilayer. New York: Garland Science; 2002. ISBN: 0-8153-3218-1, ISBN: 0-8153-4072-9
17. Włodek L. Beneficial and harmful effects of thiols. Pol J Pharmacol 2002;54:215-23.
18. Antunes F, Salvador A, Marinho HS, Alves R, Pinto RE. Lipid peroxidation in mitochondrial inner membranes. I. An integrative kinetic model. Free Radic Biol Med 1996;21:917-43.
19. James F. MINUIT Minimization package - reference manual. CERN Program Library Long Writeup D506. Geneva: CERN; 1994.
20. Saran M, Bors W. Signalling by O2-. and NO.: how far can either radical, or any specific reaction product, transmit a message under in vivo conditions? Chem Biol Interact 1994;90:35-45.
21. Fussenegger M, Bailey JE, Varner J. A mathematical model of caspase function in apoptosis. Nat Biotechnol 2000;18:768-74.
22. Legewie S, Blüthgen N, Herzel H. Mathematical modeling identifies inhibitors of apoptosis as mediators of positive feedback and bistability. PLoS Comput Biol 2006;2:e120.
23. Arbault S, Sojic N, Bruce D, Amatore C, Sarasin A, Vuillaume M. Oxidative stress in cancer prone xeroderma pigmentosum fibroblasts. Real-time and single cell monitoring of superoxide and nitric oxide production with microelectrodes. Carcinogenesis 2004; 25:509-15.
24. Kundrát P, Friedland W, Jacob P. Modelling of intercellular induction of apoptosis in oncogenic transformed cells and radiation effects on the phenomenon. Radiat Prot Dosimetry 2011;143:549–553.
25. Aguirre-Ghiso JA. Models, mechanisms and clinical evidence for cancer dormancy. Nat Rev Cancer. 2007;7:834-46.
26. Chen B, Keshive M, Deen WM. Diffusion and reaction of nitric oxide in suspension cell cultures. Biophys J 1998;75:745-54.

27. Edwards EJ, Wilson PP, Anderson MH, Mezyk SP, Pimblott SM, Bartels DM. An apparatus for the study of high temperature water radiolysis in a nuclear reactor: calibration of dose in a mixed neutron/gamma radiation field. Rev Sci Instrum 2007;78:124101.
28. Pusch M, Neher E. Rates of diffusional exchange between small cells and a measuring patch pipette. Pflugers Arch – European Journal of Physiology 1988;411:204-11.
29. Chen X, Stewart PS. Chlorine penetration into artificial biofilm is limited by a reaction-diffusion interaction. Environmental Science & Technology 1996;30:2078-83.
30. Winterbourn CC, Hampton MB, Livesey JH, Kettle AJ. Modeling the reactions of superoxide and myeloperoxidase in the neutrophil phagosome: implications for microbial killing. J Biol Chem 2006;281:39860-9.
31. Furtmüller PG, Obinger C, Hsuanyu Y, Dunford HB. Mechanism of reaction of myeloperoxidase with hydrogen peroxide and chloride ion. Eur J Biochem 2000;267:5858-64.
32. Jakopitch C, Spalteholz H, Furtmüller PG, Arnhold J, Obinger C. Mechanism of reaction of horseradish peroxidase with chlorite and chlorine dioxide. J Inorg Biochem 2008;102:293-302.
33. Furtmüller PG, Zederbauer M, Jantschko W, Helm J, Bogner M, Jakopitsch C, Obinger C. Active site structure and catalytic mechanisms of human peroxidases. Arch Biochem Biophys 2006;445:199-213.
34. Lauricella R, Allouch A, Roubaud V, Bouteiller JC, Tuccio B. A new kinetic approach to the evaluation of rate constants for the spin trapping of superoxide/hydroperoxyl radical by nitrones in aqueous media. Org Biomol Chem 2004;2:1304-9.
35. Saran M, Bors W. Radiation chemistry of physiological saline reinvestigated: evidence that chloride-derived intermediates play a key role in cytotoxicity. Radiat Res 1997;147:70-7.
36. Radi R, Beckman JS, Bush KM, Freeman BA. Peroxynitrite-induced membrane lipid peroxidation: the cytotoxic potential of superoxide and nitric oxide. Arch Biochem Biophys 1991;288:481-7.
37. Press WH, Teukolsky SA, Vetterling WT, Flannery BP. Numerical Recipes in FORTRAN: The Art of Scientific Computing (2nd ed.), Cambridge University Press, 1992. ISBN 0-521-43064-X.
38. Singh RJ, Hogg N, Joseph J, Konorev E, Kalyanaraman B. The peroxynitrite generator, SIN-1, becomes a nitric oxide donor in the presence of electron acceptors. Arch Biochem Biophys 1999;361:331-9.
39. Lomonosova EE, Kirsch M, Rauen U, de Groot H. The critical role of Hepes in SIN-1 cytotoxicity, peroxynitrite versus hydrogen peroxide. Free Radic Biol Med 1998;24:522-8.
40. Martin-Romero FJ, Gutiérrez-Martin Y, Henao F, Gutiérrez-Merino C. Fluorescence measurements of steady state peroxynitrite production upon SIN-1 decomposition: NADH versus dihydrodichlorofluorescein and dihydrorhodamine 123. J Fluoresc 2004;14:17-23.
41. Schrammel A, Pfeiffer S, Schmidt K, Koesling D, Mayer B. Activation of soluble guanylyl cyclase by the nitrovasodilator 3-morpholinosydnonimine involves formation of S-nitrosoglutathione. Mol Pharmacol 1998;54:207-12.
42. Goldstein S, Czapski G. Formation of peroxynitrite from the nitrosation of hydrogen peroxide by an oxygenated nitric oxide solution. Inorg Chem 1996;35:5935-40.
43. Lobachev V L, Rudakov E S. The chemistry of peroxynitrite. Reaction mechanisms and kinetics. Russ Chem Rev 2006;75:375-96.
44. Sigma Chemicals: Product Information – Enzymatic Assay of Myeloperoxidase (EC 1.11.1.7). Sigma Chemicals 1995; http://www.sigmaaldrich.com (downloaded 22.9.2009).
45. Sigma Chemicals: Product Information – Guaiacol (G 5502). Sigma Chemicals 2005; http://www.sigmaaldrich.com (downloaded 22.9.2009).
46. Capeillère-Blandin C. Oxidation of guaiacol by myeloperoxidase: a two-electron-oxidized guaiacol transient species as a mediator of NADPH oxidation. Biochem J 1998;336:395-404.
47. Folkes LK, Candeias LP, Wardman P. Kinetics and mechanisms of hypochlorous acid reactions. Arch Biochem Biophys 1995;323:120-6.
48. Marquez LA, Dunford HB. Chlorination of taurine by myeloperoxidase. Kinetic evidence for an enzyme-bound intermediate. J Biol Chem 1994;269:7950-6.
49. Saran M, Summer KH. Assaying for hydroxyl radicals: hydroxylated terephthalate is a superior fluorescence marker than hydroxylated benzoate. Free Radic Res 1999;31:429-36.